ERJ Express. Published on February 28, 2019 as doi: 10.1183/13993003.02020-2017

EUROPEAN RESPIRATORY *journal*

FLAGSHIP SCIENTIFIC JOURNAL OF ERS

Early View

ORiginal article

Quantitative multivolume proton-MRI in patients with cystic fibrosis lung disease: comparison with clinical indicators

Francesca Pennati, Caterina Salito, Irene Borzani, Giulia Cervellin, Simone Gambazza, Riccardo Guarise, Maria Chiara Russo, Carla Colombo, Andrea Aliverti

Please cite this article as: Pennati F, Salito C, Borzani I, *et al*. Quantitative multivolume proton-MRI in patients with cystic fibrosis lung disease: comparison with clinical indicators. *Eur Respir J* 2019; in press (https://doi.org/10.1183/13993003.02020-2017).

Quantitative multivolume proton-MRI

in patients with cystic fibrosis lung disease: comparison with clinical indicators

Francesca Pennati[1], Caterina Salito[1], Irene Borzani[2], Giulia Cervellin[2], Simone Gambazza[34], Riccardo Guarise[4], Maria Chiara Russo[4], Carla Colombo[4], Andrea Aliverti[1]

[1]Dipartimento di Elettronica, Informazione e Bioingegneria, Politecnico di Milano, Milano, Italy

[2] Fondazione IRCCS Ca' Granda Ospedale Maggiore Policlinico, Radiologia Pediatrica, Milano, Italy

[3] Fondazione IRCCS Ca' Granda Ospedale Maggiore Policlinico, U.O.C. Direzione Professioni Sanitarie, Milano, Italy

[4]Fondazione IRCCS Ca' Granda Ospedale Maggiore Policlinico, Centro Fibrosi Cistica, Milano, Italy

Address for Correspondence:

Francesca Pennati

Dipartimento di Elettronica, Informazione e Bioingegneria,

Politecnico di Milano, P.zza L. da Vinci, 32, 20133 Milano, Italy

Ph: +39 02 2399 9022

Lab: TBMLab, Via G. Colombo, 40 - 20133 Milano, Italy

ABSTRACT

Objectives: The present cross-sectional study aims to verify the relationship between quantitative multivolume magnetic resonance imaging (MRI) and clinical indicators of ventilatory abnormalities in cystic fibrosis (CF) lung disease.

Methods: 28 patients (10-27 years) with CF lung disease performed non-enhanced chest MRI, spirometry and multiple breath washout (MBW). Images acquired at end-inspiration and end-expiration were registered by optical flow to estimate expiratory-inspiratory proton density change (Δ^1H-MRI) as a measure of regional ventilation. MR images were also evaluated using a CF-specific scoring system.

Results: Biomarkers of CF ventilation impairment were defined from Δ^1H-MRI: Δ^1H-MRI median, Δ^1H-MRI quartile coefficient of variation (QCV) and percent low-ventilation volume (%LVV). Imaging biomarkers correlate to all the clinical measures of ventilation abnormalities, with the strongest correlation between Δ^1H-MRI median and forced expiratory volume in one second (FEV_1) (r^2=0.44, p<0.001), Δ^1H-MRI QCV and lung clearance index (LCI) (r^2=0.51, p<0.001) and %LVV and LCI (r^2=0.66, p<0.001). Correlations were also found between imaging biomarkers of ventilation and morphological scoring.

Conclusion: The study showed a significant correlation between quantitative multivolume-MRI and clinical indicators of CF lung disease. MRI, as a non-ionizing imaging technique, may be particularly attractive in CF care for longitudinal evaluation, providing a new imaging biomarker to detect early ventilator abnormalities.

INTRODUCTION

Lung disease is the most frequent cause of morbidity and mortality in patients with cystic fibrosis (CF) [1-2]. Since new therapies are targeting and improving outcomes in younger CF populations and in subgroups of patients with specific CF-genotype, there is an evident need for new sensitive markers of early lung changes in structure and function [3-4]. Imaging lung function and structure is particularly important in CF as functional lung changes are dissociated from structural changes [5-6]. Moreover, as CF changes are not evenly distributed within the lung, with large areas of normal lung tissue adjacent to areas of localized structural changes, imaging may reveal the structure-function relationship at regional and whole lung level [7].

Functional outcomes of CF lung disease are traditionally measured with spirometry and functional tests. Forced expiratory volume in one second (FEV_1) is the most widely used endpoint in clinical trials. Recently, forced expiratory flow at 25-75% of forced vital capacity ($FEF_{25–75}$) and forced expiratory flow at 75% of forced vital capacity (FEF_{75}) have gained new interest as markers of early lung disease, being more sensitive than FEV_1 for detecting the obstruction of the small airways [8-9]. Nevertheless, spirometry parameters have limited sensitivity for regional abnormalities and provide no information on structural impairment. Moreover, FEV_1 is effort dependent, making it unsuitable for the assessment of lung disease in patients under the age of six [10-11]. Lung clearance index (LCI), an effort independent measure of ventilation inhomogeneity derived from the multiple-breath-washout technique, has been advocated as an early sensitive marker of CF lung disease [12-13]. It has been shown that LCI is an earlier indicator of disease progression than spirometry [14] and that it correlates to structural damages [15-16]. LCI has been shown to detect treatment responses to interventions [17-18], also as a primary outcome in the context of a randomized controlled trial [19]. High resolution computed tomography (HRCT) is currently the most sensitive method of detecting and monitoring structural lung changes in CF [20-21]. However, the use of CT in pediatrics and for lifelong follow-up is restricted by cumulative radiation dose [22]. Recently, magnetic resonance imaging (MRI) has been established as a radiation-free alternative to CT to detect early structural

abnormalities of the CF lung [23-24]. HRCT and MRI scoring systems have yielded sensitive markers to quantify and characterize the structural changes at various stages of the disease [25-27]. Nevertheless, scoring systems are not routinely applied in most clinics because they are time consuming, subjective and require training. To date, no automated validated image analysis system is available to quantify the structural impairment in CF lung disease. Systems have been developed with chest CT scans to quantify trapped air [28-29] and airway/artery ratios [30] in CF studies. Similarly, there is a need to develop automated and more sensitive image analysis methods on chest MRI.

Recently, non-enhanced proton MRI has been proposed to quantify regional ventilation, by measuring differences in proton signal intensity between breath-hold images acquired in inspiration and expiration [31]. The technique has been developed to be used in a standard clinical setting, based on gradient echo acquisitions on a 1.5T MR unit [32]. The Fourier decomposition (FD) technique is an alternative method to image ventilation, which spectrally separates the signal originating from the pulmonary and the cardiac cycle in a series of 1H MR images acquired in free-breathing [33]. Multiple advances of this technique have improved the stability of the original FD method, as the matrix pencil (MP) decomposition technique [34] and the self-gated non-contrast-enhanced functional lung imaging (SENCEFUL) [35].

We assumed that breath-hold multivolume ^{1}H-MRI would provide quantitative biomarkers in CF lung disease capable of detecting functional impairment. In particular, we aimed to verify the correlation between multivolume ^{1}H-MRI biomarkers and standard clinical parameters, and to investigate the relationship between functional impairment and structural damage, quantified by a specific CF-scoring system.

MATERIALS AND METHODS

Study subjects

In this cross-sectional study, patients with CF who were admitted to their annual review in stable clinical conditions were consecutively recruited in the Lombardia Region CF Centre, University of Milan, Fondazione IRCCS Ca' Granda, Ospedale Maggiore Policlinico. Diagnosis of CF was confirmed by sweat chloride > 60 mM and/or two CF causing mutations in the CFTR gene according to established diagnostic criteria. All patients underwent chest MRI, spirometry and multiple breath washout (MBW) test as part of their annual surveillance program.

The study was approved by the local ethical committee and conducted in compliance with the guidelines of the institutional review board; written informed consent was obtained from each patient or a legal guardian.

Spirometry

Spirometry was performed on the same day as MR imaging and included the measurement of forced-expiratory volume in one second (FEV_1), forced vital capacity (FVC), forced expiratory flow at 75% of forced vital capacity (FEF_{75}), and forced expiratory flow at 25-75% of forced vital capacity (FEF_{25-75}). Values were expressed as percentage of predicted values according to the prediction equations of the Global Lung Initiative [36]. Spirometry was performed in compliance with American Thoracic Society/European Respiratory Society (ATS/ERS) guidelines [37].

Multiple Breath Washout

Multiple Breath Washout (MBW) was performed within 15 days of MR imaging. The commercial nitrogen-MBW equipment ExhalyzerD, and associated software package (Eco-Medics AG, Duernten, Switzerland) were used for data acquisition, storage and analysis in compliance with the standard operating procedure [38]. LCI was defined in compliance with the American Thoracic Society/European Respiratory Society (ATS/ ERS) consensus statement [39] as the number of lung

volume turnovers (i.e. the cumulative expired volume divided by the functional residual capacity) required to reduce the N_2 end-tidal concentration to 1/40th of the starting concentration.

^{1}H-MRI acquisition

Subjects were imaged with a 1.5T MR scanner (Magnetom AVANTO, Siemens Erlangen, Germany) at suspended full end-expiration (EXP), approximately residual volume (RV), and suspended full end-inspiration (INSP), approximately total lung capacity (TLC). The standard MR protocol routinely acquired at our institution for the follow-up of lung involvement in CF patients includes the following sequences: (1) T2-weighted half-Fourier single shot turbo spin echo (HASTE); (2) T2-weighted turbo spin echo using the periodically rotated overlapping parallel lines with enhanced reconstruction technique (TSE-PROPELLER), with end-expiratory triggered acquisition ; (3) T2-weighted balanced steady state free precession (bSSFP), acquired in free-breathing ; (4) T1-weighted 3D gradient echo (3D GRE), with breath-hold of about 6 s. Sequence parameters are reported in Table 1. All patients were used to perform respiratory maneuvers as they frequently underwent spirometric tests during their follow up. Before the imaging session they were instructed to sustain TLC and RV volumes during the scan. Images were checked by the radiologist and re-acquired within the same imaging session if they were not satisfactory.

Image processing

From top diaphragm to aortic arch, six corresponding levels were selected in the expiratory and the inspiratory T1-wighted 3D GRE scans. The images to be registered were accurately selected at the same apical-caudal level, i.e. at the same level of the airways' and vessels' trees, to minimize through-plane motion. To obtain maps of ^{1}H-density difference between the two lung volumes, the original MRI scans were processed:

1) semi-automatic lung segmentation was performed to separate lung parenchyma from the surrounding soft tissues, by using software MIPAV (Medical Image Processing, Analysis and

Visualization) [40]. Image selection and semi-automatic segmentation required about 10 minutes per patient.

2) images were normalized to the mean thoracic soft-tissue signal to quantify relative lung-signal;

3) to follow ^{1}H-signal changes between the expiratory and inspiratory images, deformable image registration (DIR), based on the optical flow algorithm [41], was applied to map corresponding pixels in the expiratory and the inspiratory image. To make the registration process more sensitive to structures rather than to overall intensity, which changes with lung volume, a Laplacian filter was applied to the images prior to DIR [32];

4) the registered images were subtracted pixel-by-pixel to provide a map of local ^{1}H-signal change between the two lung volumes (Δ^{1}H-MRI=$^{1}H_{EXP}$-$^{1}H_{INSP}$);

Values are expressed as a percentage of mean thoracic soft-tissue MRI-signal.

MR Image Analysis

MRI measures of regional ventilation. For each patient, the following MRI functional parameters were calculated across the six lung levels:

1) Δ^{1}H-MRI median;

2) Δ^{1}H-MRI quartile coefficient of variation (QCV, index of spatial heterogeneity);

3) percentage of low-ventilated volume (%LVV), as index of total ventilation defect. We defined %LVV as the percent number of pixels characterized by Δ1H-MRI<5 [42] and a) low signal magnitude in the expiratory and inspiratory images, i.e. $^{1}H\text{-}MRI_{EXP}$<10% and $^{1}H\text{-}MRI_{INSP}$<10% or b) high signal magnitude in the expiratory and inspiratory images, i.e. $^{1}H\text{-}MRI_{EXP}$>50% and $^{1}H\text{-}MRI_{INSP}$>50%. The threshold for low signal magnitude (10% of the mean thoracic soft-tissue signal) corresponds to the mean signal of the trachea across all patients.

MRI Morphological Scoring. The combination of T2- and T1-weighted sequences allows for tissue characterization. MR images were morphologically scored by a single radiologist (IB, with 8 years of experience in pulmonary MRI) at two time points (at a 12-weeks interval) in compliance with

previously published scoring systems [26-27]. The score for perfusion was excluded as contrast medium is not routinely used at our institution. All identifying information was removed and the images were read in random order. The lungs were divided into six lobar regions (five lobes plus lingula) and assessed for (i) bronchiectasis/bronchial wall thickening (bronchial wall abnormalities), (ii) mucus plugging, (iii) abscesses/ sacculations, (iv) consolidations, and (v) special findings. Findings were assessed for each individual lobe as 0 (no lobe involvement), 1 (<½ lobe involved), 2 (>½ lobe involved). Intra-reader agreement for total morphological score was assessed.

Figure 1 illustrates the steps of the overall image processing and analysis algorithm: 1) original MRI scans acquired at RV and TLC; 2) segmentation of lung parenchyma; 3) normalization of the lung parenchyma; 4) application of deformable image registration to deform the RV onto the TLC image; 5) pixel-by-pixel subtraction of the TLC image from the registered RV image to map local ^{1}H-signal change and computation of Δ^{1}H-MRI median and QCV; 6) computation of the low-ventilated volume, expressed as a percentage of the total volume.

All algorithms for image processing and quantitative analysis were implemented using custom software developed in MATLAB (The MathWorksInc, Natick, MA).

Statistical analysis

Statistical analysis was performed using SigmaStat version 11.0 (Systat Software, San Jose, CA, USA). Associations between MRI functional parameters (Δ^{1}H-MRI median, QCV and %LVV) and FEV_1, FVC, FEF_{25-75} and LCI were assessed by univariate linear regression, with determination of linear correlation coefficients (r^2). Stepwise forward regression was performed with MRI functional parameters as the dependent variables, and FEV_1, FVC, FEF_{25-75} and LCI as independent variables. Intra-reader agreement for total morphological score was assessed using Bland-Altman analysis. Univariate correlations between MRI morphological scores and FEV_1, FVC, FEF_{25-75} and LCI were

performed using Spearman's rank correlation. In order to investigate any structure-function relationship in CF lung disease, associations between Δ^1H-MRI median, QCV and %LVV and MRI score were assessed by univariate linear regression with determination of the linear correlation coefficients (r^2).

A p value <0.05 was considered statistically significant.

RESULTS

Twenty-eight consecutively selected patients (mean age 18 years, range 10-27 years, 14 males) were enrolled in the study. All subjects successfully completed the MRI protocol. Patients characteristics, spirometry and MBW are reported in Table 2. One patient was acquired twice with MRI and once with spirometry and MBW within a month and reported in the table as patient #7 and #8 (the second MR scanning was performed after two weeks of intravenous antibiotic therapy due to an exacerbation).

Comparison between MRI markers of ventilation impairment, spirometry and MBW.

In the overall population, Δ^1H-MRI median ranged from 3.9% to 17.6% and Δ^1H-MRI QCV from 0.4% to 1.4%. The total extent of low ventilation regions, i.e. %LVV, varied from 3% to 19% of total volume.

Regression analysis showed that MRI markers of ventilation impairment related with spirometric measures and LCI (Figure 2).

1) Δ^1H-MRI median positively correlated with spirometric measures and negatively with LCI, with the stronger relationship to FEV_1 (r^2=0.44, p<0.001).

2) Δ^1H-MRI QCV negatively correlated with spirometric measures and positively correlated with LCI, with the stronger relationship to LCI (r^2=0.51, p<0.001).

3) %LVV negatively correlated with spirometric measures and positively with LCI. %LVV showed the stronger relationship to LCI (r^2=0.66, p<0.001).

Results of the stepwise forward regression analysis showed FEV_1 to be the only independent predictor of Δ^1H-MRI median and LCI to be the only independent predictor of Δ^1H-MRI QCV and %LVV. Figure 3 illustrates the Δ^1H-MRI maps of four representative patients at six equally-spaced lung levels from aortic arch (I-AA) to top diaphragm (VI-TD). From panel a to d, spirometric measures decreased and LCI increased. From panel a to d, Δ^1H-MRI decreased, with values up to 20% homogeneously

distributed at all lung levels in the first patient (Fig. 2A, patient #6) and below 5% with a lot of heterogeneity in the last patient (Fig.2D, patient #20).

Figure 4 shows the %LVV maps of the four patients reported in Figure 3. Low ventilated regions were colored in blue and superimposed to the original inspiratory MR scans. From panel a to panel d, %LVV increased: 3% (patient #6); 7% (patient #21); 13% (patient #28); 18% (patient #20).

Total morphological score showed a good intra-reader agreement (mean differences 0.07, limits of agreement 2.7-2.5). In Table 3 the individual morphological MRI scores in the overall population are reported. Total score ranged from 4 to 25 with higher occurrence and severity of bronchial wall thickening/bronchiectasis and mucus plugging (respectively present in 28 and 27 patients with subscore up to 11 and 9). Correlation analysis showed that the total morphological score correlated with FEV_1, FVC, FEF_{25-75} and LCI (r^2=0.28, 0.29, 0.24 and 0.47, $p<0.01$), as well as the subscores of bronchial wall thickening/ bronchiectasis, mucus plugging and consolidation.

Relationship between MRI-score and MRI markers of ventilation.

Figure 5 reports the linear regression analysis between Δ^1H-MRI median (Fig.5A), QCV (Fig.5B) and %LVV (Fig.5C) across the six lung levels and total MRI score. With increasing MRI-score, Δ^1H-MRI median decreased (r^2=0.23, p=0.01); Δ^1H-MRI QCV increased (r^2=0.42, $p<0.001$) and %LVV increased (r^2=0.47, $p<0.001$).

DISCUSSION

This preliminary cross-sectional study evaluates the relationship between non-enhanced multivolume-MRI and clinical indicators of disease severity in CF lung disease. Results show that quantitative multivolume-MRI strongly correlates with spirometry and multiple-breath-washout technique. Over global measures of functional impairment, MRI can identify local structural and functional alterations in CF lung disease. As a non-ionizing imaging technique, quantitative multivolume MRI is particularly attractive for longitudinal evaluation in CF care.

Firstly, Δ^1H-MRI correlates to spirometry and to MBW. In CF, the progressive deterioration of lung function and the permanent structural changes result in regions with low/no gas volume change, thus in areas with low/no proton density change. If total gas volume change decreases, Δ^1H-MRI median decreases. If total gas volume change is more heterogeneously distributed, i.e. increased number of localized functional impairments adjacent to healthy lung areas, Δ^1H-MRI quartile coefficient of variation increases. This relationship is confirmed by the stronger correlation between Δ^1H-MRI median and spirometric measures, and between Δ^1H-MRI QCV and LCI.

Secondly, the extent of low-ventilated regions (%LVV) strongly correlates to LCI and moderately correlates to spirometric measures. These results are consistent with the observation that the low-ventilated lung units delay the efficiency of gas mixing (thus increasing LCI), contributing to a considerable amount of the expiratory flow limitation (thus decreasing FEV_1) [43]. Moreover, the stronger correlation between %LVV and LCI, than with spirometric measures, agrees with the hypothesis that parallel heterogeneities of specific ventilation preferentially lead to LCI increase [44]. Maps of %LVV are compatible with the very patchy ventilation images obtained by hyperpolarized gas (either ^{3}He or ^{129}Xe) MRI in adult and pediatric CF patients [45-47], but the extent of ventilation defects is lower in the present study. We attribute this difference to the higher lung volume variation between the expiratory and the inspiratory scans, necessary to better differentiate health from disease [32]. Respect to hyperpolarized gas MRI, multivolume MRI is based on straightforward pulse sequences and hardware. It does not require any gaseous tracer and can be performed on nearly any

MRI scanner as images are acquired with a standard 'gradient echo' sequence. The current image analysis is performed in 2D and requires user intervention for image selection and segmentation. In fact, the structural heterogeneity of the CF lung prevents the use of the 3D segmentation and registration algorithm [32]. Further software development, with the automatization of the segmentation algorithm, would allow automatic 3D image analysis that would be ideal for an everyday clinical use. Over global functional measurements, multivolume MRI has the advantage of identifying local structural and functional alterations, that may provide early detection ahead of LCI or spirometry and more sensitive monitoring of disease progression.

Recently, non-contrast enhanced MRI has been investigated in CF lung disease. Expiratory-inspiratory breath-hold MRI and FD-based SENCEFUL technique have reported significant differences in ventilation between CF and healthy subjects [42, 48] and among CF-specific structural impairments [42]. FD-based matrix pencil decomposition method has demonstrated associations between ventilation impairment, LCI and FEV1 [49]. Although FD-based methods take advantage of a free tidal breathing acquisition, the present approach quantifies proton signal change during a vital capacity maneuver, thus enhancing the contrast among the low ventilated regions [32, 50]. Moreover, the breath-hold acquisition minimizes artifacts related to breathing irregularities and to through-plane motion during the acquisition [34, 48].

Thirdly, our results show a moderate correlation between Δ^1H-MRI measures of ventilation and CF-specific structural score. With increasing morphological impairment, i.e. increasing CF score, gas volume change decreases and ventilation heterogeneity increases. Both CT and MRI have proven sensitivity to structural changes at various stages of the CF lung disease [51-52]. Nevertheless, previous studies have reported the presence of local functional abnormalities prior to the onset of structural injury [53]. Alterations in very small airways can result in uneven ventilation distribution, but such alterations may not be evident in MRI as structural impairment. Because the present study is cross-sectional, we can only speculate that MRI measures of ventilation will worsen with advancing structural alterations and that ventilation defects can anticipate morphological changes. Future

longitudinal studies on multivolume MRI may elucidate local structure-function relationship in patients followed over several years.

The study has some limitations. First, the study design is cross-sectional and only longitudinal data points would determine the relationship between the progression of quantitative imaging biomarkers, lung disease progression and treatment regimen.

Second, the study includes a small number of patients and lack of healthy controls. Nevertheless, the range of disease is broad enough to capture data from subjects with minimal to advanced disease and patients with minimal disease have shown median ventilation values comparable to the ones previously reported in healthy controls [32].

Third, inspiratory and expiratory MR images are not spirometer guided. To introduce quantitative multivolume MRI in the clinical practice, the implementation of lung volume guidance with a spirometer is an essential and feasible step to standardize imaging [54].

Another concern of the study is the potential for motion artifacts derived from the breath-hold requirement of 7-9 s. However, CF patients attend intensive respiratory physiotherapy programs that allow them to perform the imaging examination without difficulty, as in our group.

In conclusion, we have found a strong correlation between quantitative multivolume MRI, spirometry and multiple-breath-washout and a clear structure-function relationship in CF lung disease. These results give support to further investigating multivolume MRI to detect and regionally monitor disease progression and to quantify individual response to treatment. As a non-ionizing imaging technique multivolume MRI represents a unique tool for longitudinal studies in CF care.

REFERENCES

1. O'Sullivan BP, Freedman SD. Cystic fibrosis. Lancet 2009; 373:1891–1904.
2. Gibson RL, Burns JL, Ramsey BW. Pathophysiology and management of pulmonary infections in cystic fibrosis. Am J Respir Crit Care Med 2003; 168:918-951.
3. Wainwright CE. Ivacaftor for patients with cystic fibrosis. Expert review of respiratory medicine 2014; 8(5): 533-538.
4. Ramsey BW, Banks-Schlegel S, Accurso FJ, Boucher RC, Cutting GR, Engelhardt JF, Guggino WB, Karp CL, Knowles MR, Kolls JK, LiPuma JJ, Lynch S, McCray PB, Jr., Rubenstein RC, Singh PK, Sorscher E, Welsh M. Future directions in early cystic fibrosis lung disease research: an NHLBI workshop report. Am J Respir Crit Care Med 2012;185: 887-892.
5. Tiddens HA. Detecting early structural lung damage in cystic fibrosis. Pediatric pulmonology 2002; 34(3): 228-231.
6. De Jong PA, Nakano Y, Lequin MH, Mayo JR, Woods R, Pare PD, Tiddens HA. Progressive damage on high resolution computed tomography despite stable lung function in cystic fibrosis. European Respiratory Journal 2004; 23(1): 93-97.
7. Tiddens HA, Donaldson SH, Rosenfeld M, Paré PD. Cystic fibrosis lung disease starts in the small airways: can we treat it more effectively? Pediatric pulmonology 2010; 45(2): 107-117.
8. Bakker EM, Borsboom GJ, van der Wiel- Kooij EC, Caudri D, Rosenfeld M, Tiddens HA. Small airway involvement in cystic fibrosis lung disease: routine spirometry as an early and sensitive marker. Pediatr Pulmonol 2013; 48:1081-1088.
9. Bakker EM, Volpi S, Salonini E, van der Wiel- Kooij EC, Sintnicolaas CJ, Hop WC, Assael BM, Merkus PJ, Tiddens HA. Improved treatment response to dornase alfa in cystic fibrosis patients using controlled inhalation. Eur Respir J 2011; 38:1328-1335.
10. de Jong PA, Lindblad A, Rubin L, Hop WC, de Jongste JC, Brink M, Tiddens HA. Progression of lung disease on computed tomography and pulmonary function tests in children and adults with cystic fibrosis. Thorax 2006; 61(1): 80-85.

11. Lum S, Gustafsson P, Ljungberg H, Hulskamp G, Bush A, Carr SB, Castle R, Hoo AF, Price J, Ranganathan S, Stroobant J, Wade A, Wallis C, Wyatt H, Stocks J. Early detection of cystic fibrosis lung disease: multiple-breath washout versus raised volume tests. Thorax 2007; 62:341-347.
12. Aurora P, Bush A, Gustafsson P, Oliver C, Wallis C, Price J, Stroobant J, Carr S, Stocks J. Multiple-breath washout as a marker of lung disease in preschool children with cystic fibrosis. Am J Respir Crit Care Med 2005; 171: 249-256.
13. Aurora P, Stanojevic S, Wade A, Oliver C, Kozlowska W, Lum S, Bush A, Price J, Carr SB, Shankar A, et al. London Cystic Fibrosis Collaboration. Lung clearance index at 4 years predicts subsequent lung function in children with cystic fibrosis. Am J Respir Crit Care Med 2011; 183:752–758.
14. Kraemer R, Blum A, Schibler A, Ammann RA, Gallati S. Ventilation inhomogeneities in relation to standard lung function in patients with cystic fibrosis. Am J Respir Crit Care Med 2005; 171: 371-8.
15. Gustafsson PM, De Jong PA, Tiddens HA, Lindblad A. Multiple-breath inert gas washout and spirometry versus structural lung disease in cystic fibrosis. Thorax 2008; 63:129–134.
16. Stahl M, Wielpütz MO, Graeber SY, Joachim C, et al. Comparison of lung clearance index and magnetic resonance imaging for assessment of lung disease in children with cystic fibrosis. American journal of respiratory and critical care medicine 2017; 195(3): 349-359.
17. Davies J, Sheridan H, Bell N, Cunningham S, Davis SD, Elborn JS, Milla CE, Starner TD, Weiner DJ, Lee PS, Ratjen F. Assessment of clinical response to ivacaftor with lung clearance index in cystic fibrosis patients with a G551D-CFTR mutation and preserved spirometry: a randomised controlled trial. Lancet Respir Med 2013; 1: 630-638.
18. Amin R, Subbarao P, Lou W, Jabar A, Balkovec S, Jensen R, Kerrigan S, Gustafsson P, Ratjen F. The effect of dornase alfa on ventilation inhomogeneity in patients with cystic fibrosis. Eur Respir J 2011; 37: 806–812.

19. Ratjen F, Hug C, Marigowda G. Efficacy and safety of lumacaftor and ivacaftor in patients aged 6–11 years with cystic fibrosis homozygous for F508del-CFTR: a randomised, placebo-controlled, phase 3 trial. Lancet Respir Med 2017; 5(7): 557-567.
20. Brody AS, Klein JS, Molina PL, Quan J, Bean JA, Wilmott RW. High-resolution computed tomography in young patients with cystic fibrosis: distribution of abnormalities and correlation with pulmonary function tests. J Pediatr 2004: 145: 32–8.
21. Eichinger M, Heussel CP, Kauczor HU, Tiddens H, Puderbach M. Computed tomography and magnetic resonance imaging in cystic fibrosis lung disease. J Magn Reson Imaging 2010; 32:1370-1378.
22. O'Connell OJ, McWilliams S, McGarrigle A, O'Connor OJ, Shanahan F, Mullane D, Eustace J, Maher MM, Plant BJ. Radiologic imaging in cystic fibrosis: cumulative effective dose and changing trends over 2 decades. Chest 2012; 141:1575-1583.
23. Stahl M, Wielpütz MO, Graeber SY, Joachim C, Sommerburg O, Kauczor HU, Puderbach M, Eichinger M, Mall MA. Comparison of Lung Clearance Index and Magnetic Resonance Imaging for Assessment of Lung Disease in Children With Cystic Fibrosis. Am J Respir Crit Care Med 2016.
24. Wielpütz MO, Puderbach M, Kopp-Schneider A, Stahl M, Fritzsching E, Sommerburg O, Ley S, Sumkauskaite M, Biederer J, Kauczor HU, Eichinger M, Mall MA. Magnetic resonance imaging detects changes in structure and perfusion, and response to therapy in early cystic fibrosis lung disease. Am J Respir Crit Care Med 2014; 189:956-965.
25. De Jong PA, Ottink MD, Robben SG, Lequin MH, Hop WC, Hendriks JJ, Pare PD, Tiddens HA. Pulmonary disease assessment in cystic fibrosis: comparison of CT scoring systems and value of bronchial and arterial dimension measurements. Radiology 2004; 231:434–439.
26. Eichinger M, Puderbach M, Fink C, Gahr J, Ley S, Plathow C, et al. Contrast-enhanced 3D MRI of lung perfusion in children with cystic fibrosis-initial results. European radiology 2006; 16(10), 2147-2152.

27. Eichinger M, Optazaite DE, Kopp-Schneider A, Hintze C, Biederer J, Niemann A, Mall MA, Wielputz MO, Kauczor HU, Puderbach M. Morphologic and functional scoring of cystic fibrosis lung disease using MRI. Eur J Radiol 2012; 81:1321–1329
28. DeBoer EM, Swiercz W, Heltshe SL, Anthony MM, Szefler P, Klein R, Strain J, Brody AS, Sagel SD. Automated CT scan scores of bronchiectasis and air trapping in cystic fibrosis. Chest 2014; 145:593–603.
29. Goris ML, Zhu HJ, Blankenberg F, Chan F, Robinson TE. An automated approach to quantitative air trapping measurements in mild cystic fibrosis. Chest 2003; 123(5): 1655-1663.
30. de Jong PA, Nakano Y, Hop WC, Long FR, Coxson HO, Paré PD, Tiddens HA. Changes in airway dimensions on computed tomography scans of children with cystic fibrosis. American journal of respiratory and critical care medicine 2005. 172(2): 218-224.
31. Zapke M, Topf HG, Zenker M, et al. Magnetic resonance lung function - a breakthrough for lung imaging and functional assessment? A phantom study and clinical trial. Respir Res 2006; 7:106.
32. Pennati F, Quirk J, Yablonskiy D, Castro M, Aliverti A, Woods J. Assessment of regional lung function by multi-volume 1H-MRI in health and obstructive lung disease: comparison with 3He-MRI. Radiology 2014; 273(2): 580-590.
33. Bauman G, Puderbach M, Deimling M, et al. Non-contrast-enhanced perfusion and ventilation assessment of the human lung by means of Fourier decomposition in proton MRI. Magn Reson Med 2009; 62: 656-664.
34. Bauman G, Bieri O. Matrix pencil decomposition of time-resolved proton MRI for robust and improved assessment of pulmonary ventilation and perfusion. Magn Reson Med. 2017; 77(1): 336-342.
35. Fischer A, Weick S, Ritter CO, et al. Self-gated non-contrast-enhanced functional lung imaging (SENCEFUL) using a quasi-random fast low-angle shot (FLASH) sequence and proton MRI. NMR Biomed 2014;27(8):907–917.

36. Multi-ethnic reference values for spirometry for the 3-95-yr age range: the global lung function 2012 equations. Eur Respir J 2012; 40: 1324-43
37. Miller MR, Hankinson J, Brusasco V, Burgos F, Casaburi, et al. Standardisation of spirometry. Eur Respir J 2005; 26: 319-338.
38. Jensen R, Green K, Gustafsson P, Latzin P, Pittman J, Ratjen F, et al. Standard Operating Procedure: Multiple Breath Nitrogen Washout. 2013
39. Robinson PD, Latzin P, Verbanck S, Hall GL, Horsley A, Gappa M, Thamrin C, Arets HG, Aurora P, Fuchs S, King G, Lum S, M, Paiva M, Pillow JJ, Ranganathan S, Ratjen F, Singer F, Sonnappa S, Stocks J, Subbarao P, Thompson B, Gustafsson PM KA. ERS/ATS Consensus statement for inert gas washout measurement using multiple and single breath tests. Eur Respir J 41: 507–522, 2013.
40. About MIPAV. Center for Information Technology. National Institutes of Health. http://mipav.cit.nih.gov/. Published March 14, 2007. Updated April 5, 2013.
41. Lucas BD, Kanade T. An iterative image registration technique with an application to stereo vision. Proceeding of IJCAI 1981; 81: 674-679.
42. Pennati F, Roach DJ, Clancy JP, Brody AS, Fleck RJ, Aliverti A, Woods JC. Assessment of pulmonary structure–function relationships in young children and adolescents with cystic fibrosis by multivolume proton- MRI and CT. Journal of Magnetic Resonance Imaging 2018.
43. Verbanck S, Paiva M, Paeps E, Schuermans D, Malfroot A, Vincken W, Vanderhelst E. Lung clearance index in adult cystic fibrosis patients: the role of convection-dependent lung units. European Respiratory Journal 2013; 42(2): 380-388.
44. Aurora P, Gustafsson P, Bush A, Lindblad A, Oliver C, Wallis CE, Stocks J. Multiple breath inert gas washout as a measure of ventilation distribution in children with cystic fibrosis. Thorax 2004; 59(12): 1068-1073.

45. Kirby M, Svenningsen S, Ahmed H, Wheatley A, Etemad-Rezai R, Paterson NA, Parraga G. Quantitative evaluation of hyperpolarized helium-3 magnetic resonance imaging of lung function variability in cystic fibrosis. Academic radiology 2011; 18(8): 1006-1013.
46. Mentore K, Froh DK, de Lange EE, Brookeman JR, Paget-Brown AO, Altes TA. Hyperpolarized He 3 MRI of the lung in cystic fibrosis: assessment at baseline and after bronchodilator and airway clearance treatment1. Academic radiology 2005: 12(11): 1423-1429.
47. McMahon CJ, Dodd JD, Hill C, Woodhouse N, Wild JM, et al. Hyperpolarized 3helium magnetic resonance ventilation imaging of the lung in cystic fibrosis: comparison with high resolution CT and spirometry. European radiology 2006; 16(11): 2483-2490.
48. Veldhoen S, Weng AM, Knapp J, et al. Self-gated Non–Contrast-enhanced Functional Lung MR Imaging for Quantitative Ventilation Assessment in Patients with Cystic Fibrosis. Radiology 2016; 283(1): 242-251.
49. Nyilas S, Bauman G, Sommer G, et al. Novel magnetic resonance technique for functional imaging of cystic fibrosis lung disease. European respiratory journal 2017; 50(6); 1701464.
50. Bonnel AS, Song SMH, Kesavarju K, et al. Quantitative air-trapping analysis in children with mild cystic fibrosis lung disease. Pediatr Pulmonol 2004; 38: 396-405.
51. Ciet P, Serra G, Bertolo S, Spronk S, et al. Assessment of CF lung disease using motion corrected PROPELLER MRI: a comparison with CT. European radiology 2016; 26(3): 780-787.
52. Tepper LA, Ciet P, Caudri D, Quittner AL, Utens EM, Tiddens HA. Validating chest MRI to detect and monitor cystic fibrosis lung disease in a pediatric cohort. Pediatric pulmonology 2016; 51(1): 34-41.
53. Donnelly LF, Gelfand MJ, Brody AS, Wilmott RW. Comparison between morphologic changes seen on high-resolution CT and regional pulmonary perfusion seen on SPECT in patients with cystic fibrosis. Pediatric radiology 1997: 27(12): 920-925.
54. Salamon E, Lever S, Kuo W, Ciet P, Tiddens HA. Spirometer guided chest imaging in children: It is worth the effort! Pediatric pulmonology 2017; 52(1): 48-56.

Table 1. ^{1}H-MR imaging parameters for the acquisition sequences: (1) T2-HASTE, T2 weighted half-Fourier single-shot turbo spin-echo; (2) T2-TSE-PROPELLER, T2-weighted turbo spin echo using the periodically rotated overlapping parallel lines with enhanced reconstruction technique; (3) T2-bSSFP, T2-weighted balanced steady state free precession; (4) T1-3D GRE, T1-weighted 3D gradient echo. TR repetition time; TE echo time; TA total acquisition time.

Sequence	TR (ms)	TE (ms)	Slice Thickness (mm)	In-plane Resolution (mmxmm)	Flip Angle (degrees)	Respiratory phase	TA (s)
T2-HASTE	900	85	6	1.4x1.4	171	Insp	18
T2-TSE-PROPELLER	6000	85	6	1.1x1.1	150	Respiratory triggered at exp	126
T2-bSSFP	3.61	1.46	4	1.1x1.1	52	Free-breathing	22
T1-3D GRE	3.18	1.05	5	0.9x0.9	5	Exp, Insp	6

Table 2. Anthropometric, clinical and lung function data of patients. Patient 7 is the same as patient 8, acquired twice with MRI and once with spirometry and multiple breath washout within a month. BMI = Body mass index; FEV_1 = percent predicted forced expiratory volume in one second; FVC = percent predicted forced vital capacity; FEF_{75} = percent predicted forced expiratory flow at 75% of forced vital capacity FEF_{25-75} = percent predicted forced expiratory flow at 25-75% of forced vital capacity; LCI = lung clearance index. Bcc- Burkholderia cepacia complex, A.fum-Aspergillus fumigatus group, Ax-Achromobacter xylosoxidans, Hi-Haemophilus influenzae, Pa-Pseudomonas aeruginosa, MSSA-Staphylococcus aureus methicillin sensitive, Sm-Stenotrophomonas maltophilia, A.ver-Aspergillus versicolor, Mabsc-Mycobacterium abscessus complex, N.spp -Nocardia Spp, S.spp- Scedosporium spp, PN-Streptococcus pneumonia, A.flav-Aspergillus flavus, C.spp -Candida spp, S.marcescens- Serratia marcescens

Subject #	Age [yr]	Sex	BMI	CF genotype	Sputum culture	FEV_1	FVC	FEF_{25-75}	LCI
1	16	F	17.7	F508*del*, UN	Bcc, A.fum	49.7	71.9	15.1	16.6
2	12	F	15	F508*del*, F508*del*	Ax, Hi	54.1	62.8	27.3	23.7
3	14	F	17.7	3849+10KbC>T, 711+5G->A	Pa	47.6	60.7	27.3	13.0
4	19	F	25.1	F508*del*, F508*del*	Pa, MSSA	112.7	126.7	73.1	11.6
5	17	M	19.5	F508*del*, UN	MSSA, Pa	103.4	100.9	99.5	14.3
6	15	F	19	F508*del*, N1303K	Pa	131.2	129.5	113.9	11.1
7	17	M	21.5	G542X, G542X	MSSA, Sm, A.ver	107.6	112.1	85.3	12.7
8	17	M	21.5	G542X, G542X	MSSA, Sm, A.ver	107.6	112.1	85.3	12.7
9	16	M	16.5	F508*del*, N1303K	MSSA, Pa, Mabsc	76.9	100.2	35.0	16.7
10	17	M	17.6	5T-TG12, L61P	N.spp	48.6	82.9	17.8	13.2
11	17	F	21.4	F508*del*, F508*del*	S.spp	74.1	88.1	38.8	17.2
12	11	M	14.8	F508*del*, R1066C	Pa, PN	100.6	106.0	73.9	10.1
13	17	F	22.2	F508*del*, 3659delC	A.fum, MSSA, Pa	78.3	80.6	64.4	14.6
14	14	M	16.7	F508*del*, F508*del*	Pa, Mabsc	106.6	111.0	85.4	13.1
15	20	F	18.2	F508*del*, F508*del*	Ax, MSSA	82.1	88.5	60.5	12.9
16	13	M	15.2	F508*del*, G85E	Pa, MSSA	69.9	79.9	41.4	13.2
17	13	M	14.3	F508*del*, G85E	Pa, MSSA	64.2	76.7	32.5	14.7
18	25	M	22.9	N1303K, 2183AA->G	A.fum, Pa, A.flav	59.6	82.2	20.4	20.1
19	15	F	18.2	F508*del*, N1303K	MSSA, Sm, A.flav	55.9	93.6	17.2	21.7
20	23	M	22.6	F508*del*, F508*del*	Ax, MSSA	36.0	62.2	10.7	20.0
21	25	M	22.3	F508*del*, F508*del*	Pa	84.2	97.0	49.3	11.5
22	24	F	23.7	F508*del*, N1303K	MSSA, A.fum, A.flav	102.6	108.8	79.9	11.3
23	26	F	21.1	F508*del*, F508*del*	C.spp, A.fum	55.6	82.0	18.9	20.8
24	10	F	14.8	F508*del*, 1717-1G->A	*S.marcescens*	75.5	95.6	32.2	13.2
25	22	F	21	F508*del*, N1303K	MSSA, A.fum	79.2	95.9	37.7	14.8

26	27	M	22.6	R347P, R1066C	Ax, MSSA	60.1	93.0	24.3	16.5
27	13	F	15.6	G85E, H1375P	MSSA	103.8	98.4	119.7	8.9
28	16	M	17.9	F508*del*, G542X	MSSA, Ax, Mabsc	64.6	70.9	40.9	16.9
Mean±SD	**18±5**	**50% M**	**19.2±3.1**			**78.3±24.4**	**91.8±18.1**	**51.0±31.7**	**14.9±3.7**

Table 3. Prevalence of MRI morphological subscores [30-31] and univariate correlations between each morphological subscore and FEV_1, FVC, FEF25-75 and LCI. FEV_1 = percent predicted forced expiratory volume in one second; FVC = percent predicted forced vital capacity; FEF_{25-75} = percent predicted forced expiratory flow at 25-75%; LCI = lung clearance index. Correlation coefficient a are reported where statistically significant. *p<0.05, **p<0.01, ***p<0.001.

	Prevalence, n (%)	Score (min - max)	r^2 with FEV_1	r^2 with FVC	r^2 with FEF 25-75	r^2 with LCI
Bronchial wall thickening/ bronchiectasis	28 (100)	1 - 11	0.17*	–	0.21*	0.53***
Mucus plugging	27 (96.4)	0 - 9	0.15*	–	0.20*	0.43***
Abscesses/ sacculations	8 (28.6)	0 - 3	–	–	–	–
Consolidation	19 (67.9)	0 - 4	–	0.20*	–	–
Special findings	15 (53.6)	0 – 5	–	–	–	–
Total score	28 (100)	4 - 25	0.28***	0.29***	0.24**	0.47***

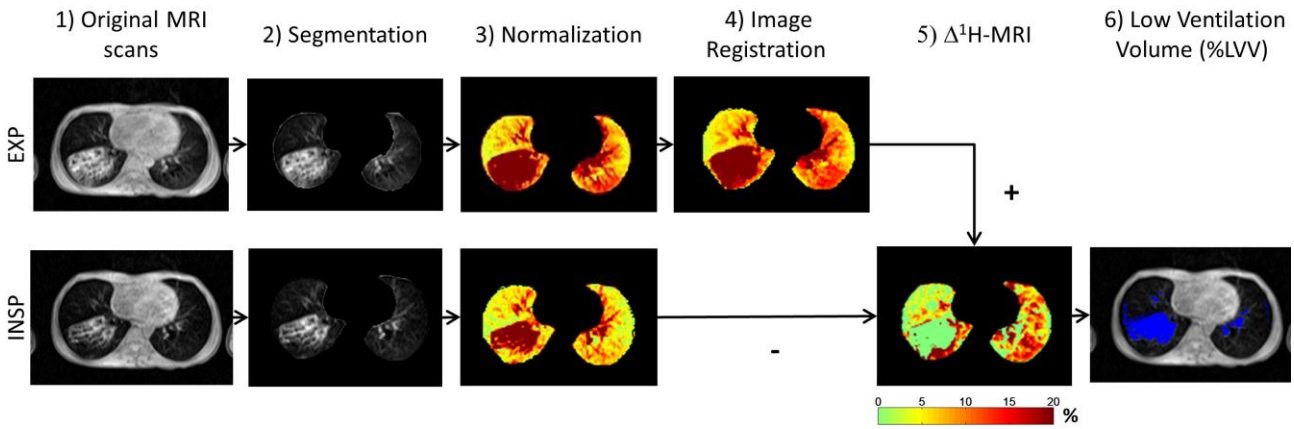

Figure 1. Image processing steps: 1) the original MRI scans acquired at suspended full end-expiration (EXP) and suspended full end-inspiration (INSP) selected at the same lung level; 2) image segmentation to extract the lungs from the surrounding tissues; 3) image normalization to mean thoracic soft-tissue signal; 4) application of deformable image registration to deform the EXP onto the INSP image; 5) pixel-by-pixel subtraction of the registered INSP image from the EXP image, to provide a map of local ^{1}H signal change between the two lung volumes ($\Delta^{1}H\text{-MRI}={}^{1}H_{EXP}-{}^{1}H_{INSP}$); 6) calculation of low-ventilation volume (in percentage to total lung volume); low-ventilated pixels are superimposed on the original INSP image as blue pixels.

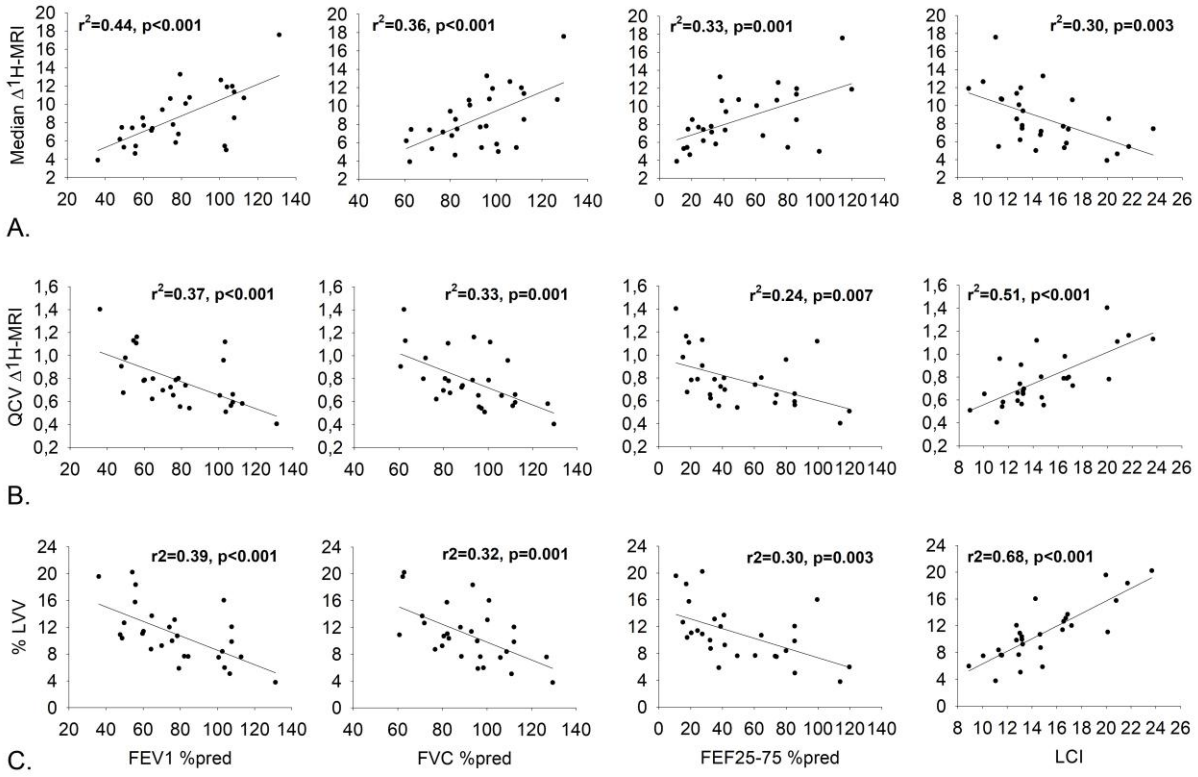

Figure 2. Results of linear regression between MRI measures of ventilation (A. Δ^1H-MRI median B. Δ^1H-MRI QCV, quartile coefficient of variation and C. %LVV, percent of low-ventilated volume) and FEV1% predicted = percent predicted forced expiratory volume in one second (I column); FVC% predicted = percent predicted forced vital capacity (II column); FEF25-75 %predicted = percent predicted forced expiratory flow at 25-75% of forced vital capacity (III column); LCI=lung clearance index (IV column). The quadratic linear correlation coefficients (r2) and p-values are reported for each graph.

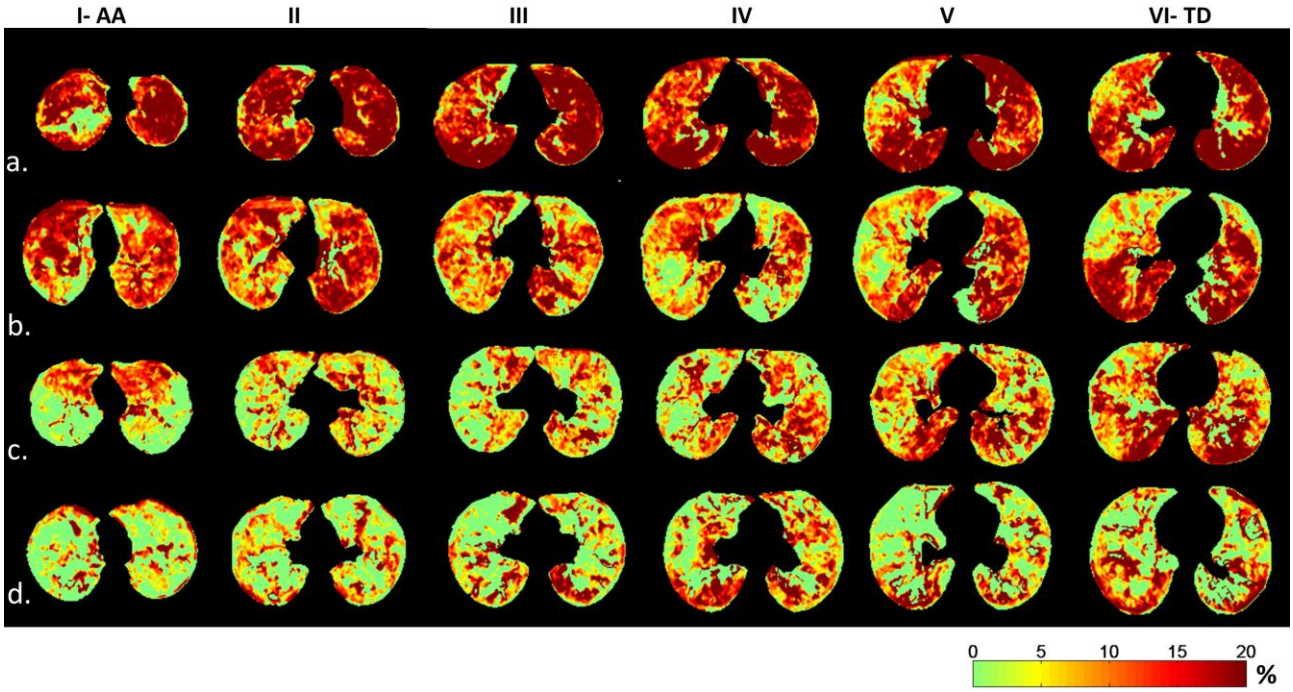

Figure 3. Proton-density change(Δ^1H-MRI) maps of four representative patients (a-d) are shown at six equally-spaced lung levels from aortic arch (I-AA) to top diaphragm (VI-TD). From panel a to panel d the patients have decreased FEV1% predicted, FVC% predicted and increased LCI.a) Patient #6, FEV1=131%, FVC=129%, LCI=11; b) patient #21, FEV1=84%, FVC=97%, LCI=11; c) patient #28, FEV1=65%, FVC=71%, LCI=17; d) patient #20, FEV1=36%, FVC=62%, LCI=20. Color spectra indicate the ^{1}H signal difference as a percentage of the mean thoracic soft-tissue signal.

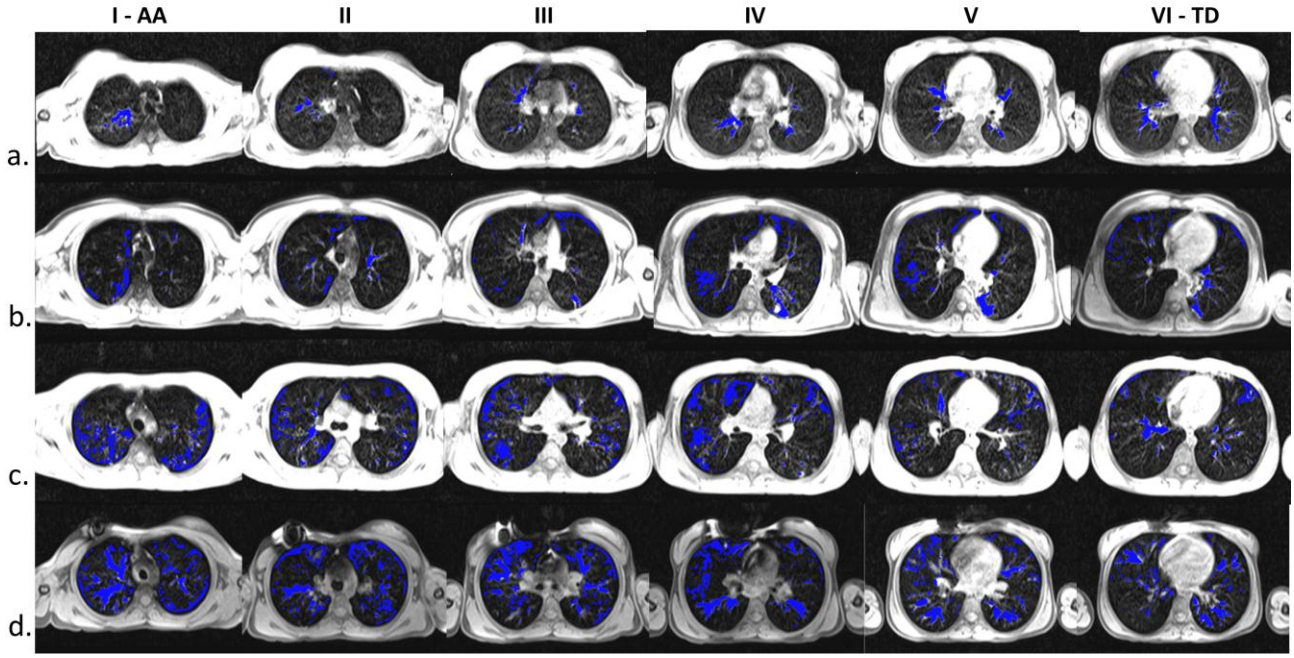

Figure 4. The low-ventilated regions of the four representative patients (a-d) shown in Figure 2 are colored in blue and superimposed to the original inspiratory MR scans at six equally-spaced lung levels from aortic arch (I-AA) to top diaphragm (VI-TD). From panel a to panel d %LVV increases: 1) 3%; b) 7%; c) 13%; d) 18%.

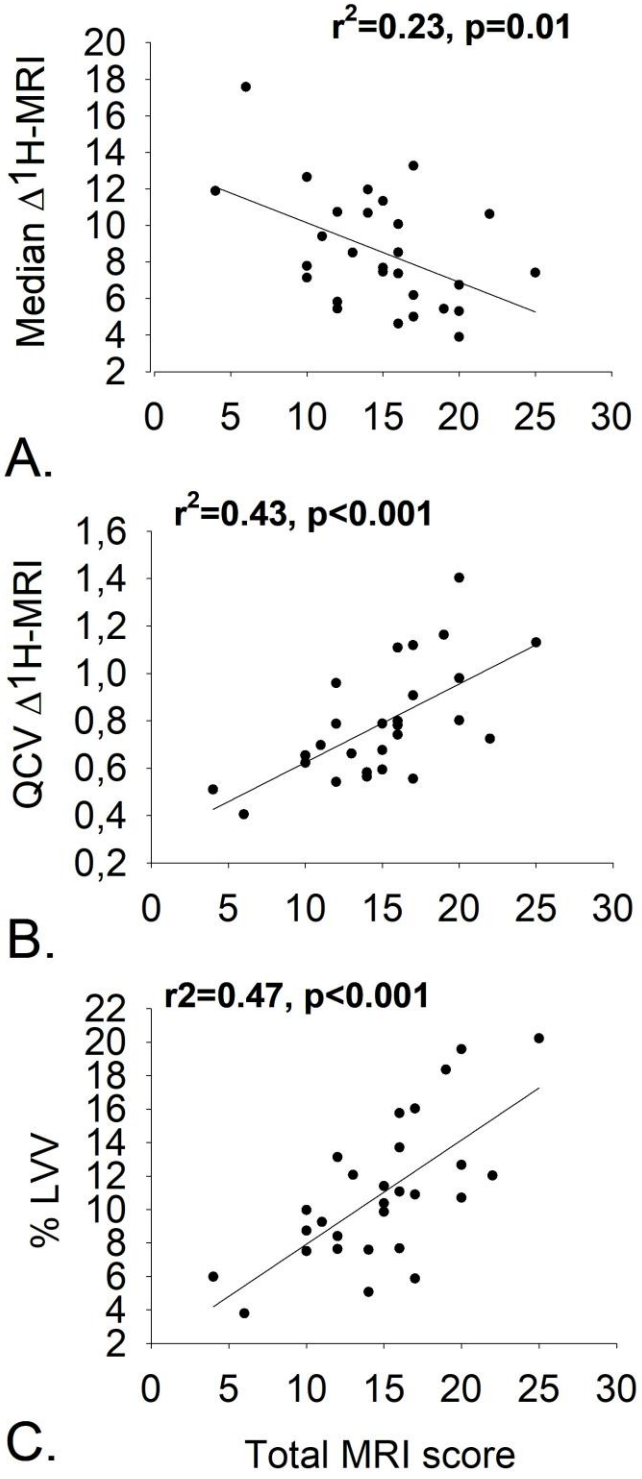

Figure 5. Correlation results between MRI measures of ventilation (A.Δ^1H-MRI median B.Δ^1H-MRI QCV, quartile coefficient of variation and C. %LVV, low-ventilated volume percentage) and MRI morphological score. The quadratic linear correlation coefficients (r2) and p-values are reported for each graph.